PUBLICATION I

Dry-etched silicon-on-insulator waveguides with low propagation and fiber-coupling losses

In: Journal of Lightwave Technology 2005.
Vol. 23, No. 11, pp. 3875–3880.

Dry-Etched Silicon-on-Insulator Waveguides With Low Propagation and Fiber-Coupling Losses

Kimmo Solehmainen, Timo Aalto, James Dekker, Markku Kapulainen, Mikko Harjanne, Kaupo Kukli, Päivi Heimala, Kai Kolari, and Markku Leskelä

***Abstract*—Optical rib waveguides with various widths and heights were fabricated on silicon-on-insulator (SOI) substrates. Silicon etching was based on dry etching with inductively coupled plasma (ICP)-type reactive ion etcher. The etching process was developed to ensure low optical losses. Propagation loss of 0.13 ± 0.02 dB/cm was measured for the fundamental mode at the wavelength of 1550 nm in a curved 114-cm-long waveguide. The reflection losses were suppressed by applying atomic layer deposition (ALD) in the growth of antireflection coatings (ARCs).**

***Index Terms*—Atomic layer deposition (ALD), integrated optics, optical device fabrication, optical losses, optical waveguides, silicon-on-insulator (SOI) technology.**

I. Introduction

THE AIM of integrated optics technology is to realize a variety of different optical components on a single chip. As a consequence of the mature and widespread state of silicon-based technology, Si substrate has served as a base for many different waveguide material systems used in integrated optics. These include, e.g., silica [1], [2], germanium [3], silicon oxynitride [4], polymers [5], and silicon-on-insulator (SOI) [6]–[11]. Also III–V semiconductors have been structured on silicon [12]. One of the main advantages of SOI waveguides is the possibility for a size reduction of integrated optical structures. This results from the high refractive index of silicon, setting a high index contrast between the silicon core and the surrounding oxide cladding. Another strong motivation to study such structures has risen from the desire to monolithically integrate SOI-based optical components and control electronics.

The fabrication of single-mode SOI waveguides with low propagation losses (~ 0.1 dB/cm) has been demonstrated using a wet silicon-etching process [7]. The production of functional integrated optical components using wet etching is difficult due to the modest critical dimension control. Dry etching offers the required anisotropic etch profile and is therefore preferred in practical applications. However, achieving low-loss SOI waveguides with dry etching is not straightforward because of the surface roughness produced on the exposed sidewalls. The surface-roughness-induced scattering of light is the key factor determining the optical losses present in the SOI waveguide. In this work, a fabrication process based on dry silicon etching was developed to produce low-loss SOI waveguides. Waveguide test structures were designed to enable accurate determination of the optical loss.

The SiO_2/Si interface present at the fiber/waveguide connection reflects 16% of the incoming light intensity, if the possible airgap is ignored. Two waveguide connections produce reflection losses of 28% (1.45 dB), which has the same order of magnitude as the other loss components present in the waveguide. The reflection losses can be reduced with an antireflection coating (ARC). Typically, this is done by sputtering layers of suitable material on the end facets after the chip is diced and polished. Atomic layer deposition (ALD) is a promising technique for the realization of optical coatings [13]. In ALD, the film is grown in a sequential manner, which basically offers nanometer accuracy in thickness control. Since ALD offers an even growth regardless of the surface shape, it enables the preparation of high-quality optical coatings also on vertical sidewalls. Thus, ALD could be used for deposition of the ARC as a wafer-level-process step, instead of being a chip-level process. In this study, the feasibility of ALD in preparation of ARCs was tested by depositing tantalum pentoxide Ta_2O_5 films on polished waveguide-end facets.

II. Waveguide Fabrication

The formation of SOI waveguides is relatively simple compared to, e.g., silica-on-silicon technology, since growth of the active layer is avoided. The necessary processing steps include only the mask patterning, silicon etching, and cladding oxide deposition. In this study, a 300-nm SiO_2 film was used beneath the resist as an additional hard mask layer. The purpose of the SiO_2 mask was to ensure the protection of the patterned structures during the Si etching. The SiO_2 deposition was done with a low-temperature-oxide (LTO) process in a low-pressure chemical-vapor-deposition (LPCVD) furnace. Waveguide patterns were transferred to the oxide mask using standard photolithography and dry oxide etching in a parallel-plate plasma etcher. Silicon etching was done using an inductively coupled plasma (ICP)-type reactive ion etcher provided by Surface Technology Systems (STS). In order to minimize the surface roughness caused by the etching step, the etching process was modified from the STS advanced silicon etch (ASE) process [14]. In the ASE process, the sidewall passivation and

Manuscript received December 23, 2004; revised March 31, 2005. This work was funded by the European Space Agency (ESA) under ESTEC/Contract No. 17703/03/NL/PA.

K. Solehmainen, T. Aalto, J. Dekker, M. Kapulainen, M. Harjanne, P. Heimala, and K. Kolari are with the VTT Information Technology, Microelectronics, FIN-02044, Finland (e-mail: kimmo.solehmainen@vtt.fi; timo.aalto@vtt.fi; james.dekker@vtt.fi; markku.kapulainen@vtt.fi; mikko.harjanne@vtt.fi; paivi.heimala@vtt.fi; kai.kolari@vtt.fi).

K. Kukli and M. Leskelä are with the Laboratory of Inorganic Chemistry, Department of Chemistry, University of Helsinki, FIN-00014, Finland (e-mail: kaupo.kukli@helsinki.fi; markku.leskela@helsinki.fi).

Digital Object Identifier 10.1109/JLT.2005.857750

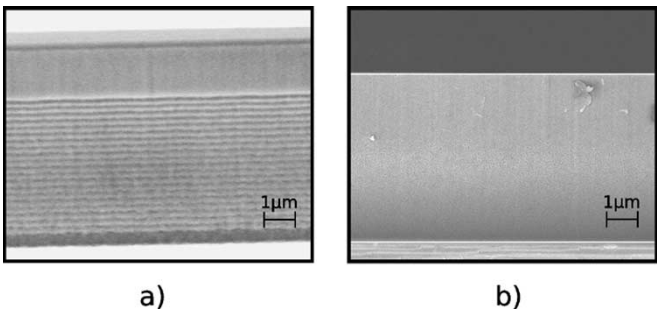

Fig. 1. SEM pictures of an etched waveguide sidewall fabricated with (a) standard ASE ICP etch process and (b) continuous-passivation ICP etch process.

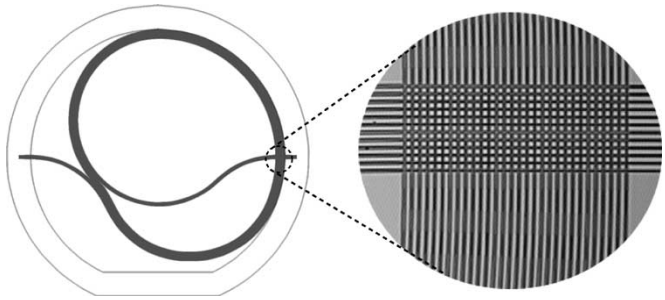

Fig. 2. Layout of the spiral waveguide mask showing a magnified microscope image of the mask section, where waveguide crossings take place. The spiral shown here includes several waveguides in parallel with different waveguide widths.

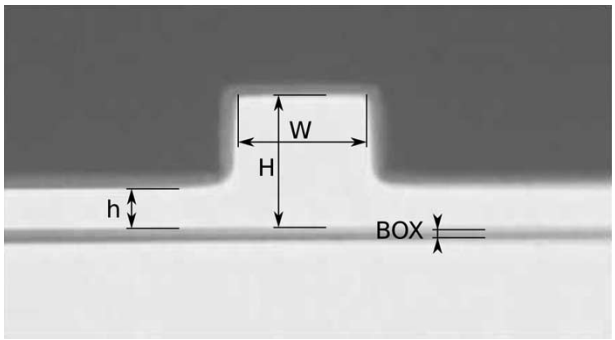

Fig. 3. Microscope photograph showing a cross section of the realized rib-waveguide structure.

silicon-etching steps are alternated subsequently. SF_6 and C_4H_8 are used as the etching and passivation gases, respectively. In this work, the passivation, which is necessary for anisotropic etching, was used continuously in the etching process. In continuous passivation, the flow rate of the passivating gas is linearly increased from its initial value as the etching deepens. The C_4F_8 flow rate was initially 120 sccm and was increased 2 sccm/min, while the SF_6 flow rate was kept constant at 40 sccm. The chamber pressure was 12 mtorr. The RF generator was operated at 13.56-MHz frequency. The power connected to the coil was constant at 600 W, while the power connected to the platen was initially 30 W and was then decreased at a rate of 1 W/min. The Si etch rate in ICP etching was 440 nm/min. The etch-depth variation over the wafer was measured with a profilometer as $\pm 7\%$. The etch selectivity against the AZ5214 resist was measured as 8:1, while the selectivity against SiO_2 was 13:1. The selectivities were significantly lower than in the typical ASE process because of the continuous passivation. In terms of surface roughness, the advantage of the continuous-passivation etch process over the standard ASE process can be seen in Fig. 1. The figure shows scanning-electron-microscope (SEM) images of the waveguide sidewalls etched with both processes. The alternating etching and passivation steps of the ASE process result in an undulated sidewall, as shown in Fig. 1(a). In principle, this undulation does not change the waveguide cross section along the direction of light propagation. However, the degree of random surface roughness of the ASE process is higher than in the continuous-passivation process shown in Fig. 1(b). After the silicon etching, the resist residuals and the oxide mask were removed with oxygen plasma stripping and wet chemical etching, respectively. The final step in the waveguide fabrication was the deposition of a 1-μm top-cladding oxide layer by wet thermal oxidation at 1050 °C.

The test structures in the mask included 114-cm-long waveguides with various widths. The long waveguides were fitted to the 10-cm wafer by constructing them in a spiral form, as seen in Fig. 2. As there were several waveguides traveling in parallel in the spiral, each waveguide passed through 100 waveguide crossings. The bending radius of these waveguides was not fixed, it varied from 2.5 to 4.2 cm along the length of the waveguide. In addition to the long curved waveguides, there were also 4-cm-long straight waveguides in the mask. They were used for studying antireflective coatings on waveguide-end facets. The waveguide geometry was of rib type (Fig. 3), which can confine large optical modes without sacrificing single-mode operation [11]. The waveguide core defined by the rib has thickness H and width W. The thickness of the slab surrounding the rib is h. The buried oxide layer (BOX) in the SOI wafers used was 1–3-μm thick. Three different SOI layer thicknesses were tested as a substrate, resulting in different waveguide thicknesses. A bond and etch-back SOI (BESOI) wafer yielded $H = 9$ μm (BOX $= 1$ μm). SOI layers of $H = 5$ μm (BOX $= 3$ μm) and $H = 2$ μm (BOX $= 3$ μm) were formed by epitaxially growing silicon on initially 1-μm thick smart-cut SOI wafers. The SOI thickness variation was measured to be ± 0.5 μm for BESOI wafers and ± 0.05 μm for the epitaxially thickened smart-cut wafers. The resistivity of the SOI layers was 1500–3500 Ωcm. For the waveguides studied here, such a high resistivity results in negligible absorption losses compared to the scattering losses. The etch depth H-h was varied in different samples, so that the ratio h/H varied between 0.5 and 0.4. The waveguide width in the mask varied between 2 and 11 μm. The lithography process and the thermal oxidation change the waveguide dimensions from the nominal values. The dimensions given in the text below are actual dimensions after the processing, verified with an optical microscope.

III. Propagation-Loss Measurements

Soref *et al.* [11] have proposed a formula for the waveguide dimensions that lead to single-mode operation in rib-type

straight waveguides:

$$\frac{W}{H} \leq 0.3 + \frac{\frac{h}{H}}{\sqrt{1-\left(\frac{h}{H}\right)^2}}. \quad (1)$$

The formula is applicable when $h/H \geq 0.5$. For the curved waveguides presented here, Soref's formula cannot be directly applied. An immediate contradiction comes from the fact that h/H was often made slightly less than 0.5 in order to minimize the bending losses. With such a slight deviation from Soref's condition, however, it is expected that one could estimate the approximate single-mode limit using the formula. This assumption has also been verified with simulations [6], [15]. Another discrepancy comes from the fact that in a curved waveguide, single-mode operation can be achieved with dimensions that would cause the corresponding straight waveguide to be multimoded. With an appropriate bending radius, the bending losses in a curved waveguide can be very high for the weakly guided higher order modes, while still very small for the fundamental mode. In that case, the curved waveguide is, in practice, single-moded, and the loss of the fundamental mode can be measured. In this study, the single-mode/multimode behavior was determined experimentally by monitoring the output of the waveguide with an IR camera while moving the input fiber in the vicinity of the waveguide input. With a waveguide showing single-mode behavior, the movement away from the optimal input-fiber alignment generates symmetrical intensity attenuation at the output, while the shape of the output intensity distribution is not changed. However, in the case of a multimode waveguide, such an input change results in variations in the output intensity distribution, which can be detected with the camera.

For the propagation-loss measurements, the waveguide ends were diced and polished to optical quality. In the measurement, unpolarized light from a broadband light source was coupled into the waveguide with a single-mode fiber. Transmitted light was coupled into another single-mode fiber and guided to an optical power meter. By replacing the power meter with an optical spectrum analyzer, the transmission spectrum could be measured. A fiber-to-fiber reference transmission was measured by directly butt coupling the input and output fibers. The propagation-loss results for one of the waveguide chips containing 114-cm-long curved SOI waveguides are shown in Fig. 4. The dimensions of these waveguides were $H = 9$ μm and $h = 4$ μm. A minimum insertion loss of 18.6 dB including propagation, bending, crossing, and fiber-coupling losses was measured at 1550 nm through a 6.7-μm-wide waveguide. The propagation losses were determined by subtracting calculated reflection and modal coupling losses of the fiber-waveguide connections from the insertion loss and dividing the remainder with the waveguide length. The reflection loss due to the two fiber-waveguide facets was calculated as 1.4 dB. Index-matching oil was used to eliminate the effect of the airgap. The modal coupling loss between the fiber and the waveguide depends on the waveguide geometry. The modal losses were defined by simulations with the commercial TempSelene software (version 4.3.04) from C2V, which calculates both the modal fields and the overlap integrals between them. For the fiber, a Gaussian field distribution with $1/e$ field radius of 5 μm was assumed. For the waveguide corresponding to the 18.6-dB insertion loss ($W = 6.7$ μm), the modal coupling loss due to two fiber couplings was simulated as 2.5 dB, yielding the propagation loss of 0.13 dB/cm. The length of the waveguides enabled accurate determination of the propagation loss, since coupling losses, which are typically difficult to estimate accurately, had only a small contribution to the result. Furthermore, the quality of the edge polishing had little effect on the results. The error in the loss measurement was estimated as $\pm$0.02 dB/cm, which is significantly more accurate than $\pm$0.3–0.5 dB/cm, typical to previous studies of SOI waveguide propagation loss [7]–[9]. As other loss components, such as misalignment loss, bending loss, and losses due to the waveguide crossings are neglected, this propagation-loss figure can be taken as a worst case approximation. The measured losses correspond to the fundamental mode only, as higher order modes had very high radiation losses along the curved waveguide. The disappearance of the higher order modes at the waveguide output was confirmed with the IR camera. After measuring several spiral waveguide chips and examining the propagation losses as a function of waveguide width, a pit-shape behavior similar to that of Fig. 4 was noticed. This behavior is consistent with previous SOI waveguide-loss studies [8]–[10]. With narrower waveguides, the intensity distribution is closer to the waveguide walls, increasing the scattering losses. As the width increases, it is expected that power leakage from the fundamental mode into the lossy higher order modes will be increased. If Soref's formula were to applied to the curved wavegu ides in Fig. 4, the width limit for single-mode operation would be $W \leq 7.2$ μm. This limit was confirmed with simulations for both straight and bent waveguides [6], [15]. The results suggest that propagation losses around 0.1 dB/cm can be achieved in single-mode straight waveguides with the current processing technology. This is the lowest propagation loss published so far in the literature for a dry-etched SOI waveguide.

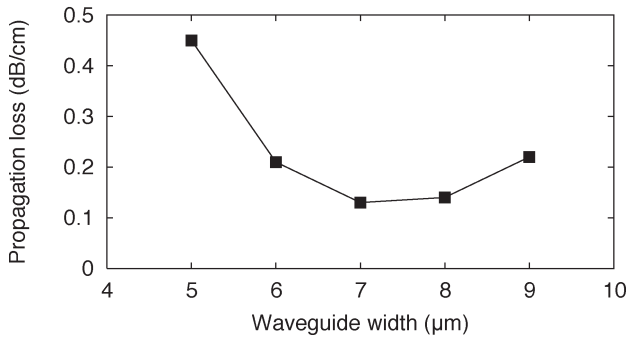

Fig. 4. Results of the propagation-loss measurements for a 114-cm-long curved SOI rib waveguide.

The propagation-loss spectrum was measured in the wavelength range of 1150–1650 nm for three waveguides with different thicknesses. The dimensions of these waveguides are shown in Table I. Because of higher losses, the measurements had to be performed on 7-cm-long straight waveguides for the waveguides with $H = 5.0$ and 2.0 μm. The results are shown in Fig. 5. As seen in the figure, the propagation loss increases

TABLE I
DIMENSIONS OF THE WAVEGUIDES USED IN THE PROPAGATION-LOSS MEASUREMENT

H (μm)	h (μm)	W (μm)	Length (cm)
9.0	4.0	6.7	114
5.0	2.5	4.4	7
2.0	1.0	3.6	7

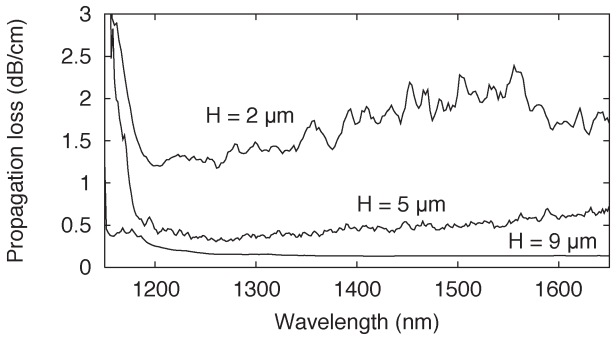

Fig. 5. Measured transmission spectra for SOI waveguides with various waveguide heights.

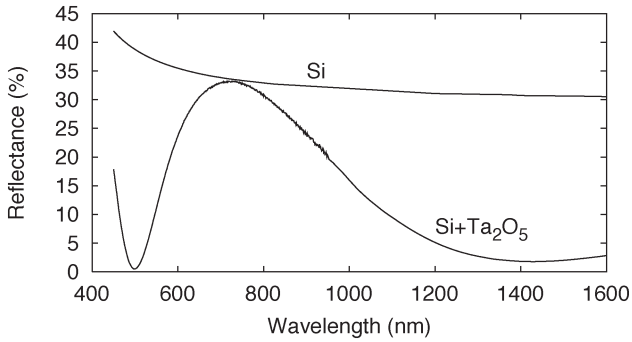

Fig. 6. Measured reflectance spectrum of an Si surface and an Si surface covered with 170 nm of Ta_2O_5.

TABLE II
MEASURED REFRACTIVE INDEX OF Ta_2O_5 GROWN WITH ALD

Wavelength (nm)	Refractive index
633	2.15
830	2.12
1300	2.11
1550	2.10

significantly as the waveguide thickness is decreased. This is a result of increased sensitivity to surface roughness with smaller waveguide dimensions. The fabrication process was optimized only for approximately 10-μm-thick SOI waveguides. Therefore, the propagation losses of thinner SOI waveguides are expected to decrease by further process optimization. As the waveguide dimensions decrease, spectra are also prone to distortions. The periodic fluctuations are probably due to interruptions in the waveguide structure originating from the fabrication process. As expected, below 1200 nm, the material absorption of Si increases the optical losses rapidly, making the material opaque. As long as the propagation losses caused by the waveguide structure are kept low, the Si material itself allows the use of a wide wavelength range from approximately 1.3 to 4 μm [16].

IV. ANTIREFLECTION COATING (ARC)

One of the main issues in any integrated optical-waveguide technology is the connection between the waveguide and an optical fiber, resulting in reflection, modal coupling, and fiber misalignment losses. In order to eliminate the reflection losses at the interface between the Si waveguide and an optical fiber, Ta_2O_5 ARCs were deposited with ALD on the waveguide-end facets. Ta_2O_5 was chosen as the antireflection material because it is transparent at the wavelengths of interest and its refractive index is known to be close to the optimum, which is 2.26 for the SiO_2/Si interface. The ALD apparatus used here was not designed for the wafer-level processing. Therefore, the deposition was done on the waveguide chips after polishing the chip facets. Amorphous Ta_2O_5 coatings were deposited at a temperature of 300 °C from $Ta(OC_2H_5)_5$ and H_2O [17] using 6500 growth cycles. A FilmTek 4000 fiber-optic-based spectrophotometer from Scientific Computing International was used to measure the film thickness and the refractive index of these layers. The setup did not allow the direct measurement of the waveguide-end facets. Therefore, the measurements were carried out on a reference surface. Fig. 6 shows the measured reflectance spectra of a blank Si substrate and Si substrate coated with Ta_2O_5. A thickness of 170 nm was solved from the reflectance spectrum for the Ta_2O_5 film. Measured refractive indexes for ALD-grown Ta_2O_5 at discrete wavelengths are given in Table II. Being away from the ideal thickness of 185 nm, the wavelength of minimum reflectance is shifted from the targeted 1550 nm to 1430 nm. The deviation from the targeted value was not due to thickness-control accuracy. Instead, it was a result of lack of calibration in the deposition process, a deprivation that can easily be eliminated in the future work. Despite the fact that the thickness was not ideal, the reflectance at 1550 nm was decreased from 30.5% of bare Si to 2.4% for Ta_2O_5-coated Si surface. The measurement shown was for air/Si and air/ARC/Si structures. The calculations showed that a 170-nm-thick layer of ALD-grown Ta_2O_5 reduces the reflection losses due to two fiber connections from 1.45 to 0.07 dB.

The impact of the ARC on the coupling losses was determined in the loss measurements. The insertion losses of straight 4-cm-long waveguides were measured before and after the ARC deposition. In the measurement, light was coupled into the waveguide with a single-mode fiber. The transmitted light was gathered with a multimode fiber. Index-matching oil was used to fill the air gaps between the fibers and the waveguide. The Ta_2O_5 coating decreased the losses significantly. On the average, the loss reduction after the Ta_2O_5 ARC deposition was measured as 1.6 ± 0.3 dB. This value is substantially close to the calculated value of 1.4 dB, which assumes a Ta_2O_5 ARC 170 nm in thickness. The difference between the simulated and measured value is within the accuracy of the insertion-loss measurement.

V. Conclusion

The fabrication of low-loss dry-etched silicon-on-insulator (SOI) rib waveguides was described. Propagation loss of 0.13 ± 0.02 dB/cm was measured at 1550 nm for a 114-cm-long curved waveguide. The measurement accuracy was exceptionally good. This is the lowest value reported in the literature for a dry-etching-based SOI waveguide and among the lowest reported in SOI material. Spectral measurements showed that the losses remained below 0.2 dB/cm from 1230 to 1750 nm. Reflection losses of 1.4 dB present at the waveguide/fiber interface were eliminated by growing Ta_2O_5 antireflection coatings (ARCs) on waveguide-end facets with atomic layer deposition (ALD).

References

[1] T. Miya, "Silica-based planar lightwave circuits: Passive and thermally active devices," *IEEE J. Sel. Topics Quantum Electron.*, vol. 6, no. 1, pp. 38–45, Jan.–Feb. 2000.

[2] E. M. Yeatman, M. M. Ahmad, O. McCarthy, A. Vannucci, P. Gastaldo, D. Barbier, D. Mongardien, and C. Moronvalle, "Optical gain in Er-doped SiO_2-TiO_2 waveguides fabricated by the sol-gel technique," *Opt. Commun.*, vol. 164, no. 1–3, pp. 19–25, Jun. 1999.

[3] S. Fama, L. Colace, G. Masini, G. Assanto, and H. C. Luan, "High-performance germanium-on-silicon detectors for optical communications," *Appl. Phys. Lett.*, vol. 81, no. 4, pp. 586–588, Jul. 2002.

[4] R. M. de Ridder, K. Worhoff, A. Driessen, P. V. Lambeck, and H. Albers, "Silicon oxynitride planar waveguiding structures for application in optical communication," *IEEE J. Sel. Topics Quantum Electron.*, vol. 4, no. 6, pp. 930–937, Nov.–Dec. 1998.

[5] R. Yoshimura, H. Nakagome, S. Tomaru, and S. Imamura, "Fabrication of single-mode polymeric optical waveguides by laser-beam writing," *Electron. Lett.*, vol. 31, no. 25, pp. 2169–2171, Dec. 1995.

[6] T. Aalto, M. Harjanne, M. Kapulainen, P. Heimala, and M. Leppihalme, "Development of silicon-on-insulator waveguide technology," in *Proc. SPIE*, San Jose, CA, 2004, vol. 5355, pp. 81–95.

[7] U. Fischer, T. Zinke, J.-R. Kropp, F. Arndt, and K. Petermann, "0.1 dB/cm waveguide losses in single-mode SOI rib waveguides," *IEEE Photon. Technol. Lett.*, vol. 8, no. 5, pp. 647–648, May 1996.

[8] A. G. Rickman, G. T. Reed, and F. Namavar, "Silicon-on-insulator optical rib waveguide loss and mode characteristics," *J. Lightw. Technol.*, vol. 12, no. 10, pp. 1771–1776, Oct. 1994.

[9] J. Schmidtchen, A. Splett, B. Schüppert, and K. Petermann, "Low loss singlemode optical waveguides with large cross-section in silicon-on-insulator," *Electron. Lett.*, vol. 27, no. 16, pp. 1486–1488, Aug. 1991.

[10] T. Zinke, U. Fischer, A. Splett, B. Schüppert, and K. Petermann, "Comparison of optical waveguide losses in silicon-on-insulator," *Electron. Lett.*, vol. 29, no. 23, pp. 2031–2033, Nov. 1993.

[11] R. A. Soref, J. Schmidtchen, and K. Petermann, "Large single-mode rib waveguides in GeSi-Si and Si-on-SiO_2," *IEEE J. Quantum Electron.*, vol. 27, no. 8, pp. 1971–1974, Aug. 1991.

[12] Z. H. Zhu, F. E. Ejeckam, Y. Qian, J. Zhang, Z. Zhang, G. L. Christenson, and Y. H. Lo, "Wafer bonding technology and its applications in optoelectronic devices and materials," *IEEE J. Sel. Topics Quantum Electron.*, vol. 3, no. 3, pp. 927–935, Jun. 1997.

[13] T. Suntola, J. Antson, A. Pakkala, and S. Lindfors, "Atomic layer epitaxy for producing EL-thin films," in *Proc. SID Symp. Dig. Tech. Papers*, San Diego, CA, May 1980, pp. 108–109.

[14] A. M. Hynes, H. Ashraf, J. K. Bhardwaj, J. Hopkins, I. Johnston, and J. N. Shepherd, "Recent advances in silicon etching for MEMS using the ASE process," *Sens. Actuators*, vol. 74, no. 1–3, pp. 13–17, 1999.

[15] T. Aalto. (2004, Dec.). Microphotonic silicon waveguide components. Ph.D. dissertation, Dept. Electr. and Commun. Eng., Helsinki Univ. Technol. [Online]. Available: http://www.vtt.fi/inf/pdf/publications/2004/P553.pdf

[16] E. D. Palik, *Handbook of Optical Constants of Solids*. New York: Academic, 1985.

[17] K. Kukli, M. Ritala, and M. Leskelä, "Atomic layer epitaxy growth of tantalum oxide thin films from $Ta(OC_2H_5)_5$ and H_2O," *J. Electrochem. Soc.*, vol. 142, no. 5, pp. 1670–1675, May 1995.

Kimmo Solehmainen received the M.Sc. Tech. degree, major in microelectronics, from Helsinki University of Technology, Finland, in 2000. He is currently pursuing the doctorate degree focusing on the subject of fabrication technology for integrated optics.

He has worked at VTT, Helsinki since 2001. His interests include microelectronics fabrication methods, optical device characterization, and spectrophotometric measurement techniques.

Timo Aalto received the M.Sc. Tech. and D.Sc. Tech. degrees in optoelectronics from Helsinki University of Technology, Finland, in 1998 and 2004, respectively.

He has worked at VTT, Helsinki, since 1997. His research interests are the design, simulation, fabrication, and characterization of silicon-based waveguides, especially silicon-on-insulator (SOI) waveguides.

James Dekker received the B.Sc. degree in Mechanical Engineering and the Ph.D. degree in materials science from the University of California at Davis in 1990 and 1997, respectively.

From 1997 to 1999, he held a postdoctoral position at Tampere University of Technology, Tampere, Finland, where he characterized defects in epitaxial III–V alloys. From 1999 to 2001, he worked at Helsinki University of Technology, characterizing defects in semiconductors and insulators. Since then, he has been at VTT, Helsinki, where he develops fabrication processes for microelectromechanical-system (MEMS) devices.

Markku Kapulainen received the M.Sc. Tech. degree in physics from Helsinki University of Technology, Finland, in 2001.

Since 2001, he has worked at VTT, Helsinki, as a Research Scientist. His interests include optical measurement techniques, fiber optics, and free-space optics.

Mikko Harjanne received the M.Sc. Tech. degree in optoelectronics from Helsinki University of Technology, Finland, in 2003.

Since his graduation, he worked at the Optoelectronics Laboratory of Helsinki University of Technology. He joined VTT, Helsinki, in 2005.

Kaupo Kukli received the Ph.D. degree from the University of Tartu, Tartu, Estonia, in 1999.

From 1996 to 1997, he was a Researcher at Helsinki University of Technology, Helsinki, Finland. Since 1998, he has worked as a Researcher both at the University of Helsinki and at the University of Tartu.

Päivi Heimala received the M.Sc. and Lic.Ph. degrees in physics from the University of Helsinki, Finland, in 1990 and 1993, respectively.

She is currently the Group Manager of the Photonics Group at VTT, Helsinki.

Kai Kolari received the M.Sc. degree in physics from the University of Helsinki, Finland, in 1999.

From 1999 to 2000, he was with Fortum Oyj, where he developed solar cell technology. He currently works as a Research Scientist at VTT, Helsinki, where his main interest is biomicrofluidics.

Markku Leskelä received the D.Sc. Tech. degree in 1980 from Helsinki University of Technology, Finland.

During 1980–1986, he worked as an Associate Professor at the University of Oulu, Finland, and during 1986–1990, as a Professor at the University of Turku, Finland. Since 1990, he has held the present position of Professor of Inorganic Chemistry at the University of Helsinki, Finland.